CRISPR-Cas immunity repressed by a biofilm-activating pathway in *Pseudomonas aeruginosa*

Adair L. Borges#, Bardo Castro#, Sutharsan Govindarajan, Tina Solvik, Veronica Escalante, Joseph Bondy-Denomy*

Department of Microbiology & Immunology and the Quantitative Biosciences Institute, University of California, San Francisco, San Francisco, CA 94143

#Equal contribution

*Corresponding author: joseph.bondy-denomy@ucsf.edu

CRISPR-Cas systems are adaptive immune systems that protect bacteria from bacteriophage (phage) infection. To provide immunity, RNA-guided protein surveillance complexes recognize foreign nucleic acids, triggering their destruction by Cas nucleases. While the essential requirements for immune activity are well understood, the physiological cues that regulate CRISPR-Cas expression are not. Here, a forward genetic screen identifies a two-component system (KinB/AlgB), previously characterized in regulating *Pseudomonas aeruginosa* virulence and biofilm establishment, as a regulator of the biogenesis and activity of the Type I-F CRISPR-Cas system. Downstream of the KinB/AlgB system, activators of biofilm production AlgU (a σ^E orthologue) and AlgR, act as repressors of CRISPR-Cas activity during planktonic and surface-associated growth. AmrZ, another biofilm activator, functions as a surface-specific repressor of CRISPR-Cas immunity. *Pseudomonas* phages and plasmids have taken advantage of this regulatory scheme, and carry hijacked homologs of AmrZ, which are functional CRISPR-Cas repressors. This suggests that while CRISPR-Cas regulation may be important to limit self-toxicity, endogenous repressive pathways represent a vulnerability for parasite manipulation.

Clustered regularly interspaced short palindromic repeats (CRISPR) and CRISPR-associated (cas) genes are RNA-guided nucleases found in nearly half of all bacteria[1]. CRISPR-Cas systems are mechanistically diverse, with six distinct types (I-VI) identified, based on signature genes, mechanisms of action, and the type of nucleic acid target[1]. Our strong understanding of the basic components to enable sequence specific DNA

35 and RNA cleavage have enabled functional transplantation into heterologous bacterial[2,3]
36 and eukaryotic[4,5] hosts. Given that many Cas proteins encode nucleases[6] the fine-tuned
37 regulation of these systems to avoid toxicity is likely a key factor to enable safe retention
38 of a CRISPR-Cas immune system[7]. Multiple signals have been shown to activate
39 CRISPR-Cas function in diverse organisms, such as quorum sensing[8,9], temperature[10],
40 membrane stress[11,12], altered host metabolite levels[13,14], and phage infection[15-18].
41 However, relatively little is known regarding the factors and/or signals that serve to
42 temper CRISPR-Cas activity and mitigate the risk of acquiring and expressing a
43 nucleolytic immune system.
44
45 Type I CRISPR-Cas systems are comprised of a multi-subunit RNA-guided surveillance
46 complex, a trans-acting nuclease (Cas3)[19-21], and proteins dedicated to spacer
47 acquisition, Cas1 and Cas2[22,23]. *Pseudomonas aeruginosa* has become a powerful
48 model organism for studying Type I CRISPR-Cas mechanisms[24-29], functions[3,23,30,31],
49 evolution[32-34], and interactions with phages utilizing anti-CRISPR proteins[35-38]. The *P.*
50 *aeruginosa* strain PA14 possesses an active Type I-F CRISPR-Cas immune system that
51 naturally targets many phages. The surveillance complex is composed of four Cas
52 proteins (Csy1, Csy2, Csy3, and Csy4), which are encoded together in a single
53 operon[26]. The surveillance complex is guided by CRISPR RNAs (crRNAs) originating
54 from one of two chromosomally encoded CRISPR arrays[26]. Finally, a separate operon is
55 responsible for the production of Cas1 and a Cas2-3 fusion protein, the latter of which
56 mediates nucleolytic destruction of target DNA.
57
58 To discover regulators controlling the expression of the CRISPR-Cas surveillance
59 complex in *P. aeruginosa*, we utilized a *P. aeruginosa* strain PA14 engineered to
60 express *lacZ* in place of the *csy3* gene (*csy3::lacZ*)[39]. The *csy3*::*lacZ* reporter strain was
61 subjected to transposon mutagenesis and colonies isolated and screened on X-gal
62 plates. ~40,000 colonies were visually examined for increased or decreased levels of β-
63 galactosidase. Multiple independent insertions were identified that abolished LacZ levels
64 within *lacZ* and upstream genes (*csy1* and *csy2*), indicating successful mutagenesis and
65 screening. Thirty distinct mutants with transposon insertions outside of this region, with
66 altered β-galactosidase levels, were isolated and mapped. These mutants are listed in
67 Supplementary Table 1 with β-galactosidase levels quantified for mutants that grew well
68 in culture. Four independent insertions were identified in a single gene, *kinB*, which

resulted in apparent mucoidy plating morphology and decreased β-galactosidase production (Supplementary Fig. 1a). Quantification of β-galactosidase levels in liquid growth experiments revealed ~50% less *csy3::lacZ* expression compared to wild-type (WT) PA14 for each mutant (Supplementary Table 1, Supplementary Fig. 1b). We focused on *kinB* (a sensor kinase/phosphatase) because it was the only gene with >1 independent transposon insertion and displayed the largest β-galactosidase activity change.

To determine the consequences of *kinB* disruption and decreased *csy* expression on CRISPR-Cas function, we measured the ability of *kinB::Tn* insertions to limit the replication of phage, when introduced into a wild-type strain background. Phages used to assay activity are: DMS3$_{acrIE3}$ which is an untargeted control phage, DMS3m$_{acrIE3}$ [40], which is fully targeted by the PA14 Type I-F CRISPR-Cas system, and phage DMS3m$_{acrIF4}$, which is partially targeted, by virtue of encoding a "weak" anti-CRISPR, *acrIF4,* that binds to the surveillance complex to inhibit CRISPR-Cas function[35,37,41]. The *kinB::Tn* strains remained resistant to DMS3m$_{acrIE3}$ infection, but DMS3m$_{acrIF4}$ formed 10-fold more plaques relative to WT, demonstrating attenuated CRISPR-Cas function (Figure 1a, Supplementary Fig. 1c). This defect was complemented by expression of *kinB in trans* (Supplementary Fig. 1c). Growth of control phage DMS3$_{acrIE3}$ was not impacted in the absence of KinB (Figure 1a). Furthermore, two other targeted phages, JBD26 (naturally possessing *acrIF4*) and JBD25 (a partially targeted phage with no Acr) also showed increased replication in the *kinB:Tn* strain (Supplementary Fig. 1d) relative to WT PA14. Replication of a phage with a weak anti-CRISPR or one that is targeted by a less active spacer is therefore a sensitive barometer for perturbations in CRISPR-Cas levels. Together, these data confirm that in the absence of *kinB, csy* gene expression and phage targeting are decreased.

KinB is a sensor kinase/phosphatase in a two-component system with response regulator AlgB. The KinB/AlgB system has a large regulon within *P. aeruginosa*, but is well-known for its role in biofilm regulation[42]. In the absence of KinB function, the activity of the transcription factor AlgU (a σ^E orthologue and an activator of biofilm formation) is enhanced[43,44]. This activation of AlgU manifests solely due to the lack of KinB phosphatase activity and the resulting accumulation of the phosphorylated form of the response regulator AlgB (P-AlgB). The phosphorylation of AlgB has been attributed to

103 unknown kinases[45,46] (Fig. 1b). The resulting accumulation of P-AlgB activates the
104 periplasmic protease AlgW (a DegS homolog), which degrades MucA, liberating sigma
105 factor AlgU[47,48,49] (Fig. 1b). AlgU positively regulates many factors involved in biofilm
106 production, including AlgR, AlgD, AlgB, and AmrZ[50-52].
107
108 To determine if this KinB-controlled biofilm activation pathway also regulates CRISPR-
109 Cas immunity, we tested the ability of phosphatase and kinase dead KinB mutants to
110 complement an in-frame Δ*kinB* deletion, using the replication of the partially-targeted
111 DMS3m$_{acrIF4}$ phage as a metric for CRISPR-Cas activity. WT *kinB* or kinase inactive
112 H385A *kinB* complemented the CRISPR defect (Fig. 1c), indicating KinB kinase activity
113 is dispensable for CRISPR-Cas activation. However, a P390S *kinB* mutant incapable of
114 dephosphorylating the response regulator AlgB did not complement, and in fact
115 decreased CRISPR-Cas activity further (Fig. 1c). This suggests that CRISPR-Cas
116 expression is inhibited by the accumulation of P-AlgB. A Δ*kinB*Δ*algB* double mutant
117 restored CRISPR-Cas targeting to WT levels (Supplementary Fig. 2a), confirming the
118 role of this signaling pathway. A strain lacking *algB* (Δ*algB*) or possessing a D59N
119 mutant that cannot be phosphorylated had elevated CRISPR-Cas activity, supporting the
120 repressive role of P-AlgB (Supplementary Fig. 2b). Together, these data suggest that
121 KinB-mediated dephosphorylation of AlgB lifts CRISPR-Cas inhibition, and conversely
122 accumulation of high levels of P-AlgB (achieved in Δ*kinB* or *kinB P390S*) leads to
123 CRISPR-Cas repression.
124
125 To assess CRISPR-Cas regulation downstream of P-AlgB, anti-phage immunity was
126 assayed in Δ*algU* and Δ*algR* backgrounds, revealing enhanced targeting of DMS3m$_{acrIF4}$
127 but not control phage DMS3$_{acrIE3}$ in each knockout (Fig. 1d). Complementation with *algR*
128 and *algU* restored CRISPR-Cas levels in their respective knockout backgrounds (Fig.
129 1d). This demonstrates that these proteins repress CRISPR-Cas immunity. Double
130 knockouts of each gene combined with Δ*kinB* each resembled the respective Δ*algU* and
131 Δ*algR* single knockouts, consistent with these factors acting downstream of KinB
132 (Supplementary Fig. 2a). The observed plaquing defects seen with the DMS3m$_{acrIF4}$
133 phage are CRISPR-dependent, as double knockouts (*kinB, algB, algU, algR* mutants
134 combined with *csy3::lacZ*) revealed plaquing equivalent to *csy3::lacZ* alone
135 (Supplementary Fig. 2c).
136

137 Phages that use anti-CRISPRs to inhibit CRISPR-Cas immunity must cooperatively
138 infect the same cell in order to produce a sufficient dose of anti-CRISPR to permit phage
139 replication[41,53]. The multiplicity of infection (MOI) required to overwhelm immunity is
140 dependent on the affinity of the anti-CRISPR for the CRISPR-Cas machinery and the
141 intracellular concentration of CRISPR-Cas components. To understand how this
142 regulatory pathway controls phage cooperation requirements on a population level by
143 potentially shifting the intracellular concentration of CRISPR-Cas complexes, liquid
144 cultures of Δ*algU* and Δ*kinB* mutants were infected with a virulent derivative of phage
145 DMS3m$_{acrIF4}$ at both high (where the WT cells are sensitive) and low (where the WT cells
146 are resistant) MOI (Figure 1e). The Δ*algU* mutant was able to limit phage replication
147 relative to WT and continue growing when infected with concentration of phages
148 sufficiently high to overwhelm WT immunity (10^6 PFU), indicating increased levels of
149 CRISPR-Cas machinery (Fig 1e). Conversely, when infected with a low MOI of phages
150 (10^4 PFU), all bacterial genotypes grew to high cell density, however the Δ*kinB* mutant
151 permitted increased phage replication relative to WT, demonstrating a decreased level of
152 immune system components (Fig. 1f). Importantly, these changes in phage replication
153 requirements were not seen in the absence of CRISPR-Cas immunity, as phage
154 replication in double knockouts *algU csy3::lacZ and kinB csy3::lacZ* resembles
155 *csy3::lacZ (*Supplementary Fig. 3a-d, f). In contrast, Δ*algR* demonstrated CRISPR-
156 independent phage resistance during liquid culture infection, and phage cooperation
157 requirements could not be reliably measured for this mutant (Supplementary Fig. 3e).
158 Taken together, these data demonstrate that a well-characterized biofilm activation
159 pathway controlled by alternate sigma factor, AlgU, represses CRISPR-Cas immunity in
160 *P. aeruginosa.*
161
162 Our screen focused on finding regulators of the *csy* operon, however the recruited Cas3
163 nuclease (encoded in a separate, nearby operon) is also an important player in Type I
164 CRISPR-Cas immunity. To measure the relative impact of the KinB/AlgB pathway in
165 controlling Cas3 and Csy complex levels, we fused an N-terminal sfCherry tag to the
166 endogenous *csy1* or *cas3* gene in the mutant backgrounds. We observed decreased
167 levels of both Cas3-sfCherry and Csy1-sfCherry in Δ*kinB* and increased levels in Δ*algR*
168 and Δ*algU* relative to WT, demonstrating that this pathway controls the levels of both
169 Cas3 and the Csy complex in the bacterial cell (Fig. 2a).

170 As Cas3-sfCherry was expressed at low levels relative to Csy1-sfCherry, and is also
171 known to be subject to post-translational control by Cas1[28], we sought to dissect the
172 relative contribution of nuclease versus surveillance complex disregulation in driving the
173 immune phenotypes of the KinB/AlgB pathway mutants. To specifically measure the
174 anti-phage activity of the Csy complex, we developed a Cas3-indepedent bioassay to
175 read out the activity of the surveillance complex in the cell. Through the rational design
176 of crRNAs to target an early phage promoter (P_E_1, P_E_2), we observed inhibition of
177 phage replication in a *P. aeruginosa* strain with a nuclease dead Cas3 ($Cas3_{D124A}$, Fig.
178 2a). This CRISPR-based transcriptional interference (CRISPRi) effect was also seen
179 when infecting with a phage that expressed the inhibitor of Cas3 recruitment, AcrIF3, but
180 not an inhibitor that blocks Csy complex-phage DNA binding[37], AcrIF1 (Fig. 2b).
181 CRISPRi was mediated by crRNAs targeting phage promoters, including one (P_E_2) that
182 completely limited phage replication in the absence of Cas3 activity, while an ORF-
183 targeting crRNA (ORF_1) was ineffective (Fig. 2b). We selected P_E_1 as a moderately-
184 functional CRISPRi spacer and expressed it in various mutant backgrounds generated in
185 this study. We observed decreased CRISPRi activity against phage $DMS3m_{acrIF3}$ in the
186 ΔkinB background, but increased CRISPRi-mediated phage repression in Δ*algR* and
187 Δ*algU,* (Fig. 2c), demonstrating that modulation of *csy* gene expression by this pathway
188 is sufficient to impact phage targeting, in a Cas3-independent manner. We conclude that
189 while the KinB/AlgB pathway regulates both Cas3 and Csy complex levels, repression of
190 surveillance complex biogenesis alone represents a powerful mechanism by which the
191 KinB/AlgB pathway controls CRISPR-Cas immunity.
192
193 AlgU and AlgR are proteins that regulate hundreds of genes in *P. aeruginosa*[54-56],
194 ultimately repressing acute virulence factors (e.g. pyocyanin) and activating chronic
195 virulence factors (e.g. biofilm production). To identify downstream CRISPR-Cas
196 regulators, we considered the large AlgU regulon[56], but focused on a factor involved in
197 biofilm production, whose expression is AlgU-dependent, *amrZ*[51,57]. AmrZ is a ribbon-
198 helix-helix type transcription factor, and acts as both a repressor and activator of
199 transcription in *Pseudomonas*[58]. We generated a knockout of *amrZ* and observed a
200 CRISPR-dependent decrease in $DMS3m_{acrIF4}$ plaque formation (Fig. 3a, Supplementary
201 Fig. 2c). This was complemented when *amrZ* was expressed *in trans* (Fig. 3a), indicating
202 that AmrZ is also a repressor of CRISPR-Cas immunity. However, when we measured
203 phage cooperation requirements in the Δ*amrZ* strain, phage replication and immune

204 protection did not differ substantially from WT (Fig. 3b,c). The most obvious difference
205 between the phage plaque assay and the assay to measure phage cooperation is that a
206 plaque assay is performed on solid plates whereas phage cooperation requirements
207 were measured in liquid culture. To test if AmrZ was a surface-specific repressor of
208 CRIPSR-Cas immunity, we measured the levels of Csy complex during surface
209 association and planktonic growth in WT and Δ*amrZ* cells using an endogenous *csy1-*
210 *sfCherry* reporter. In WT cells, the levels of Csy complex were attenuated during
211 surface-association relative to planktonic growth, but in the absence of AmrZ, Csy
212 complex levels during surface association increased to levels comparable to those in
213 planktonic growth (Fig. 3d). Deletion of *amrZ* did not impact Csy complex levels during
214 planktonic growth (Fig. 3e). To artificially increase the levels of AmrZ during planktonic
215 growth, we ectopically expressed AmrZ from a high copy plasmid. In this scenario, high
216 levels of AmrZ were sufficient to completely inhibit Csy complex expression, suggesting
217 that low AmrZ activity in planktonic growth underlies its surface-specific control of
218 CRISPR-Cas (Fig. 3f). In contrast to AmrZ, overexpression of the AlgU moderately
219 impacted Csy complex levels and AlgR was unable to repress *csy1-sfCherry* when
220 overexpressed (Fig. 3f). This is likely because AlgU and AlgR are master regulators and
221 many redundant mechanisms are in place to control their activity. Taken together, these
222 data demonstrate that AmrZ is a surface-specific repressor of the *csy* operon.

223 We next considered if phages and other mobile genetic parasites naturally antagonized
224 by CRISPR-Cas immunity had evolved mechanisms to manipulate this repressive
225 pathway. Inspired by the discovery of a *Paraburkholderia* phage that carried a distant
226 homolog of AmrZ[59], we searched the NCBI database for AmrZ homologs on
227 *Pseudomonas* mobile genetic elements (MGE). Excitingly, we identified 14 diverse
228 *Pseudomonas* genetic parasites carrying AmrZ homologs (Supplementary Table 2).
229 These MGEs included obligately lytic and temperate Myoviridae, temperate
230 Siphoviridae, and plasmids. AmrZ has been structurally characterized in complex with
231 operator DNA[58], and these mobile AmrZ homologs showed perfect conservation of
232 critical DNA-interacting residues in the ribbon-helix-helix domain, suggesting conserved
233 binding specificity (Fig. 4a, b, red residues/arrowheads). To test if these mobilized AmrZ
234 variants were capable of regulating CRISPR-Cas activity in *Pseudomonas aeruginosa*,
235 we synthesized 6 MGE-borne *amrZ* homologs and tested them for their ability to
236 complement the Δ*amrZ* strain. 5/6 homologs complemented the Δ*amrZ* mutant,

237 indicating they were active in the PA14 transcriptional network and were *bona fide* AmrZ
238 orthologs (Fig. 4c). Next, each gene was expressed in WT cells carrying an endogenous
239 *csy1-sfCherry* reporter, revealing 3 *P. aeruginosa* phage homologs ($amrZ_{PaBG}$, $amrZ_{phi3}$,
240 $amrZ_{JBD68}$) that inhibited Csy complex biogenesis at varying efficiencies (Fig. 4d). This
241 suggests the possibility that *amrZ* has been hijacked for its capacity to inhibit CRISPR-
242 Cas expression. Thus, *amrZ* acts on both sides of the battle between bacteria and
243 mobile genetic elements.
244
245 **Discussion**

246 The factors that govern expression of bacterial processes are highly variable across
247 species, reflecting niche-specific adaptations. CRISPR-Cas immune systems limit the
248 replication of foreign genetic elements, but few reports address how the regulation of
249 CRISPR-Cas impacts phage targeting. Here, we utilized a genetic screen that identified
250 KinB as a positive regulator of CRISPR-Cas function in *P. aeruginosa.* This sensor
251 kinase/phosphatase operates in a two-component system with AlgB that regulates a
252 well-characterized biofilm-stimulatory pathway, though the ligand for KinB remains
253 unknown. Removal of KinB or inactivation of its phosphatase activity leads to the
254 accumulation of P-AlgB, which stimulates the activity of CRISPR-Cas repressors AlgU,
255 AlgR, and AmrZ. This pathway is well-studied due to the recurrent isolation of alginate-
256 overproducing (mucoid) *P. aeruginosa* from the lungs of cystic fibrosis patients, with
257 mutations in *mucA*[60] and *kinB*[47,61] that lead to the constitutive activation of AlgU. This
258 biofilm pathway generates the characteristic mucoidy phenotype of CF *P. aeruginosa*
259 isolates[43,62,63], which we also observed in *kinB:Tn* mutants (Supplementary Fig. 1a).

260 This pathway is well described in its capacity to activate biofilm production, and here we
261 show that this transcriptional network also functions to dampen CRISPR-Cas activity in
262 non-biofilm conditions. In WT cells, KinB phosphatase activity increases CRISPR-Cas
263 function, though the effect is relatively mild in our experimental conditions. Relieving
264 transcriptional repression via deletion of *algU* or *algR* however leads to a hyper-
265 activation of the CRISPR-Cas immune response. We further demonstrate that *amrZ* acts
266 in this pathway to specifically repress CRISPR-Cas when cells are surface-associated,
267 leading to lower levels of Csy complex during surface-association relative to planktonic
268 growth. Phages and plasmids have taken advantage of this regulatory scheme, and
269 some *Pseudomonas* genetic parasites carry hijacked copies of the CRISPR-Cas

270 repressor *amrZ*. We show that these mobilized *amrZ* homologs retain their capacity to
271 transcriptionally repress CRISPR-Cas, demonstrating a dual role for this gene in the
272 host-pathogen arms race between bacteria and their parasites.
273
274 Considering the physiology of *P. aeruginosa* can put these findings into context with a
275 phage and CRISPR-Cas-centric view. During exponential growth is when we and others
276 observe CRISPR-Cas activation[8,9], and is also when phage infection risk is likely high
277 (i.e. metabolically active, well-mixed planktonic culture[33]). Conversely, surface-
278 association lessens phage infection risk, as spatial structure limits phage dispersal and
279 prevents a phage bloom from overtaking the entire bacterial population[64]. Though we do
280 not measure phage sensitivity in a biofilm here, biofilm production likely provides an
281 even greater level of intrinsic phage resistance, due to high levels of spatial stratification
282 and abundant polysaccharide secretion.

283 Supporting our proposal that *P. aeruginosa* surface-association/biofilm formation and
284 CRISPR-Cas expression are inversely correlated are two independent observations: **i)**
285 Our analysis of a previously published PA14 RNAseq data set[65] and proteomic data set[66]
286 revealed activation of CRISPR-Cas expression in exponential phase, and strong
287 transcriptional repression during stationary phase and biofilm growth (Supplementary
288 Fig. 4a). Interestingly Cas proteins are still detected in stationary phase and biofilm
289 growth, suggesting the cells retain some immune-competency even after transcriptional
290 shutdown (Supplementary Fig. 4b). **ii)** Previous studies on the *P. aeruginosa* CRISPR-
291 Cas system have revealed that the genome is hyper-sensitive to CRISPR-induced DNA
292 damage during surface-association and biofilm formation, leading to cell death when a
293 mismatched prophage sequence target is present in the chromosome[30,31]. This suggests
294 that CRISPR auto-immunity costs are also dependent on the growth state and physical
295 environment of the cell, and that CRISPR-Cas regulation in *P. aeruginosa* is tuned to
296 reflect this intrinsic sensitivity.

297 Here, we report the identification of a CRISPR-Cas repressive pathway in *P. aeruginosa*.
298 Phages bearing distinct anti-CRISPRs are employed in bioassays to read out the activity
299 of the CRISPR-Cas surveillance complex. Using a CRISPRi phage-repression assay,
300 coupled with translational reporters, we conclude that *algU*, *algR*, and *amrZ* control the
301 production of the CRISPR surveillance complex (Csy complex), which is where the
302 screen was focused. Cas3 levels, though low, are also modulated by the KinB/AlgB

303 pathway. Interestingly, our observations show that CRISPR-Cas activity in *P. aeruginosa*
304 does not operate at full strength, despite the capacity of a hyper-activated immune
305 system to severely limit the replication of phages relying on anti-CRISPRs for survival.
306 We speculate that the ability to control CRISPR-Cas activity during lifestyle transitions
307 may be essential for *P. aeruginosa* to safely maintain a CRISPR-Cas system by limiting
308 self-toxicity. Furthermore, we reveal an unexpected cost to negative regulation of
309 CRISPR-Cas immunity in our discovery of MGE-encoded CRISPR-Cas repressors:
310 though CRISPR-Cas control is likely essential for safe retention of the immune system,
311 the evolution of potent mechanisms of CRISPR-Cas repression has created an Achilles
312 Heel that is exploited by genetic parasites.

313 **Acknowledgements**
314 We thank members of the Bondy-Denomy lab for conversations and support relating to
315 this project. We also thank Kristine Trotta (Seemay Chou's lab, UCSF) for assistance
316 and advice in the development of fluorescent reporter assays, and Andrew Santiago-
317 Frangos (Blake Wiedenheft's lab, MSU) for advice and consultation. The Bondy-Denomy
318 lab was supported by the University of California, San Francisco Program for
319 Breakthrough in Biomedical Research, funded in part by the Sandler Foundation, and an
320 NIH Office of the Director Early Independence Award (DP5-OD021344), and
321 R01GM127489. We thank Deborah Hung's lab for providing Δ*kinB,* Δ*algR,* Δ*algU* strains
322 and associated mutants, and George O'Toole's lab providing the *csy3::lacZ* PA14 strain.
323

324 **Author Contributions**
325 J.B.D., A.L.B, and B.C. formulated study design and plans. A.L.B. designed and
326 conducted bacteriophage plaque assays, liquid infection assays, and CRISPRi assays,
327 performed CRISPR-Cas expression profiling, and conducted bioinformatics analyses.
328 B.C. conducted the genetic screen, isolated and constructed bacterial mutants,
329 conducted LacZ expression profiling, and performed bacteriophage plaque assays. S.G.
330 designed, constructed, and validated sfCherry reporter strains. T.S. conducted CRISPRi
331 assays and V.E. assisted in establishing fluorescent reporter assays. J.B.D. and A.L.B
332 wrote the manuscript.
333

334 **Competing Interests**

335 J.B.-D. is a scientific advisory board member of SNIPR Biome and Excision
336 Biotherapeutics and a scientific advisory board member and co-founder of Acrigen
337 Biosciences.
338
339 **Materials & Correspondence**
340 Correspondence should be directed to joseph.bondy-denomy@ucsf.edu
341
342 **Methods**
343 **Bacterial strains and bacteriophages.** *P. aeruginosa* UCBPP-PA14 (PA14) strains
344 and *E. Coli* strains (Sup. Table) were grown on lysogeny broth (LB) agar or liquid at 37
345 ^{o}C. Media was supplemented with gentamicin (50 µg ml^{-1} for *P. aeruginosa* and 30 µg ml^{-}
346 ^{1} for *E. Coli*) to maintain the pHERD30T plasmid or carbenicillin (250 µg ml^{-1}) for *P.*
347 *aeruginosa* or ampicillin (100 µg ml^{-1}) for *E. coli* containing the pHERD20T plasmids.
348 pHERD plasmids were induced with 0.1% arabinose. Bacteriophages stocks were
349 prepared as described previously[40]. In brief, 3 ml of SM buffer was added to plate
350 lysates of the desired purified bacteriophage and incubated at room temperature for 15
351 minutes. SM buffer containing phages was collected and 100 µl of chloroform was
352 added. This was centrifuged at 10,000 x g for 5 minutes and supernatant containing
353 phages was transferred to a screw cap storage tube and incubated at 4 ^{o}C.
354
355 **Tn mutagenesis screen.** The *csy*::*lacZ* reporter strain was subjected to transposon
356 mutagenesis and colonies were isolated on plates containing X-gal (5-bromo-4-chloro-3-
357 indolyl-β-D-galactopyranoside). ~50,000 colonies were visually examined for increased
358 or decreased levels of β-galactosidase and insertions mapped by semi-random PCR. To
359 conduct transposon mutagenesis, overnights of PA14 *csy3::lacZ* and *E. coli* containing
360 the pBTK30 Tn suicide vector were mixed in a 1:2 ratio (donor : recipient) for
361 conjugation. A second control group containing PA14wt and *E. Coli* containing the
362 pBTK30 Tn suicide vector was set up in parallel. Mixed cells were centrifuged at 4,000 x
363 g for 10 minutes to pellet cells. 100 µl of resuspended conjugation pellet was then
364 spotted on LB agar plates and incubated at 37 ^{o}C for 6hrs. Conjugation spots were
365 collected and resuspended in LB liquid media. Conjugation was then screened on an LB
366 agar plates supplemented with nalidixic acid (30 µg ml^{-}1) and gentamicin (50 µg ml^{-1}).
367 Surviving colonies containing Tn insertions were collected into 1ml of LB liquid media.
368 Serial dilution of were prepared and plated on LB agar plates supplemented with x-gal

369 (200 µg ml^{-1}) and gentamicin (50 µg ml^{-1}) and nalidixic acid (30 µg $ml^{-}1$). Plates were
370 incubated at 37 ^{o}C for 24 hours to allow for colonies to change color. Colonies displaying
371 changed expression levels as compared to our positive control (PA14 csy3::lacZ no
372 pBTK30) were then isolated onto secondary LB agar plates with X-gal and gentamicin
373 and nalidixic acid at the stated concentrations. Genomic DNA (gDNA) was collected
374 from isolated single colonies by resuspending bacterial colonies in 0.02% SDS and
375 boiling the sample for 15 minutes. Samples were then centrifuged at 10,000 x g and
376 supernatants containing gDNA were collected. Semi-random PCR was then performed
377 using PCR primers listed on sup table_. PCR samples were sequenced and reads were
378 then matched to the *P. aeruginosa* UCBPP-PA14 genome using BLAST. Isolated
379 containing genes of interest were saved as stocks (s. table 1). Transcription changes
380 were then verified via modified β-galactosidase assay.
381
382 **Plaque assays.** Plaque assays were performed on LB agar plates (1.5% agar) with LB
383 top agar (0.7% agar), both supplemented $MgSO_4$ (10 mM final concentration) and
384 gentamicin (50 µg ml^{-1}) as needed for plasmid maintenance. Spot titrations were done by
385 mixing 150 µl of a *P. aeruginosa* overnight culture with 3 ml of top agar, which was
386 dispersed evenly on a LB $MgSO_4$ plate. 3 µl of 10-fold phage dilutions were then spotted
387 on the surface. Plates were incubated overnight at 30 ^{o}C. To count plaques, full plate
388 assays were used, except when CRISPR-targeting was so strong that discrete plaques
389 could not be accurately measured. In this case, spot titrations are shown. For full plate
390 assays, 3 µl of the selected phage dilution was incubated with 150 µl of *P. aeruginosa*
391 overnight for 15 minutes at 37 ^{o}C. 3 ml of top agar was then added and the mixture was
392 dispersed evenly on a LB $MgSO_4$ plate. Individual plaques were then counted to assess
393 differences in plaquing efficiency.
394
395 **β-galactosidase assay.** A modified version of the previously described β-galactosidase
396 assay was used to measure *lacZ* activity in transcriptional fusions. Bacterial cultures
397 were grown overnight at 37 ^{o}C. Cultures were then diluted 1:100 into LB liquid medium
398 supplemented with the desired antibiotic. Diluted cultures were then incubated at 37 ^{o}C
399 until the desired time point was reached. Culture density was measured with a
400 spectrophotometer (OD_{600}) and 200 µl of the sample was added 800 µl to
401 permeabilization solution (components listed in sup table XX). Cells were mixed via
402 inversion and vortexed for 1 minute to permeabilize the cells. 200 µl of ONPG (4 mg ml^{-}

403 [1]) was added and samples were incubated for 27 minutes at 30 °C. Enzymatic reaction
404 was stopped by addition of 300 µl of 1M Na_2CO_3. Samples were centrifuged at 13,000 x
405 g for 5 minutes to remove debris and 200 µl of supernatant was moved to a 96-well plate
406 to read absorbance at 420 nm and at 550 nm. Miller units were calculated using the
407 Miller equation. 3 technical replicates per sample per experiment.
408
409 **Phage transduction of *kinB::Tn* alleles.** Transposon insertions in *kinB* from a
410 *csy3::lacZ* background were transduced into WT PA14 to enable testing of CRISPR-Cas
411 function with the same transposon insertion. Phage phiPA3 was used to infect the donor
412 strain (*csy3::lacZ, kinB::Tn*), on plates with top agar overlays, using ~10^4 PFU to
413 generate near confluent lysis. Plates were soaked in 3-4 mL of phage SM buffer and 2
414 mL collected over chloroform, vortexed, and pelleted to isolate transducing phage in the
415 supernatant. Lysates were used to infect recipient strains (WT PA14). ~10^8 PFU were
416 used to infect a culture at an MOI of 1. After 30 minutes of static incubation on the
417 bench, cultures were gently shaken at 37 °C for 20 min and then pelleted at 5000 x g.
418 Cells were washed twice with LB, and subsequently incubated at 37 °C for 1 hour to
419 allow recombination and gentamicin resistance outgrowth. Cultures were pelleted and
420 resuspended in 200 µL of LB, and plated on LB plates containing gentamicin. Controls
421 included uninfected cells and cells infected with phages not propagated on a gentamicin
422 resistant donor strain. Additionally, phage lysate was directly plated under selection to
423 confirm no residual donor strain in the phage preparation. Plates were incubated
424 overnight at 37 °C and their identity (i.e. CRISPR-Cas intact) confirmed with a plaque
425 assay using DMS3m as the target phage and PCR of the kinB locus.
426
427 **Introduction of *csy3::lacZ P. aeruginosa* UCBPP-PA14 strains.** The *lacZ* gene was
428 introduced into PA14 strains of interest via homologous recombination. Recombination
429 vector containing lacZ flanked by homology arms matching csy2 and csy4 was
430 introduced via conjugation. PA14 strains and *E. coli* containing vector were mixed at a
431 ratio of 1:2 (recipient:donor). Mixture was heat shocked at 42 °C for 10 min. Mating spot
432 was then plated on a LB agar plate and incubated overnight for 30 °C. Mating spot was
433 then collected, resuspended in 1 ml of LB liquid media and plated on VBMM plates
434 supplemented with 50 ug/mL gentamicin to select for colonies with the integrated
435 homology plasmid. Colonies were cultured overnight in LB in the absence of selection at
436 37 °C, and were then diluted and counterselected on no salt LB (NSLB) agar plates

437 supplemented with 15% sucrose. Surviving colonies were then grown on LB agar plates
438 supplemented with gentamicin and X-gal to check for *lacZ* insertion via color change and
439 lacZ insertion was further verified via PCR.
440
441 **Generation of an PA14*ΔamrZ* strain using the endogenous I-F CRISPR-Cas**
442 **system.** Complementary oligonucleotides encoding a crRNA targeting the *amrZ* gene of
443 PA14 were annealed and ligated into the multiple cloning site of the pHERD30T vector.
444 A fragment possessing homology arms flanking the desired mutation (500 bp upstream
445 and 500 bp downstream) around *amrZ* was cloned into a distinct location (NheI site) of
446 the same vector via Gibson assembly. The new plasmid containing both a crRNA and
447 homology region was introduced into WT PA14 via electroporation. Transformation
448 efficiency dropped dramatically in the presence of the crRNA due to the toxicity caused
449 by self-targeting. All surviving colonies had the desired clean deletion of the *amrZ* gene.
450 Deletions were confirmed by PCR of the region of interest and subsequent Sanger
451 sequencing of the amplicon. A 2000 bp region flanking *amrZ* was PCR amplified and
452 sequencing primers were designed to sequence both the deletion junction and outside of
453 the original 500 bp flanking regions to confirm the removal of the *amrZ* gene.
454
455 **Liquid phage cooperation assay**. Liquid phage infections were performed as
456 described in[41]. In brief, an overnight culture of cells was diluted 1:100 into fresh media,
457 and infected with virulent phage DMS3m$_{acrIF4}$ in biological triplicate in a 96 well Costar
458 plate. Cells were incubated at 37 ^{o}C with constant rotation and OD600 measured every 5
459 minutes in a Biotek H4 Synergy plate reader. Phage were harvested from each well and
460 quantified by plaque assay after 24 hours. In these experiments, all strains used in the
461 assay carried 2 spacers against the DMS3m$_{acrIF4}$ phage to prevent phage escape: one
462 endogenous spacer (CRISPR2_sp1), and the other spacer was provided on a
463 pHERD30T plasmid.
464
465 **Generation of endogenous Csy1-sfCherry and Cas3-sfCherry reporters**
466 Endogenous Csy1-sfCherry and Cas3-sfCherry reporters were constructed similar to the
467 construction of *csy3::lacZ.* We initially verified that tagging of sfCherry at the N terminus
468 of Csy1 and Cas3 are functional, when expressed from a plasmid. pMQ30-sfCherry-
469 Csy1, which contains sfCherry sequence flanked by 657 bp upstream of csy1 and 701
470 bp downstream of *csy1* start codon, was cloned in pMQ30 plasmid between HindIII and

471 BamHI sites using Gibson assembly. pMQ30-sfCherry-Cas3, which contains sfCherry
472 sequence flanked by 353 bp upstream of cas3 and 350 bp downstream of cas3 start
473 codon, was cloned in pMQ30 plasmid between HindIII and BamHI sites using Gibson
474 assembly. 4 bp that overlap between the end of *cas1* and the beginning of *cas3* were
475 duplicated in the final construct. Both pMQ30-sfCherry-Csy1 and pMQ30-sfCherry-Cas3
476 contains ggaggcggtggagcc sequence (encoding GGGGA) as linker between sfCherry
477 and the respective tagged proteins. The Csy1-sfCherry and Cas3-sfCherry construct
478 were introduced into PA14 strains of interest via homologous recombination. Strains
479 containing appropriate insertion were verified via PCR.
480
481 **sfCherry reporter profiling**. **Liquid**: Cells were diluted 1:100 from an overnight culture
482 into fresh LB (with antibiotics and inducer if required), and grown for the indicated
483 number of hours in biological triplicate. 500 µl of each sample was then spun down at
484 8,000xg for 2 minutes, and resuspended in 500 µl of M9 media. Samples were loaded in
485 to a 96 well plate (150 µl /well) in technical triplicate and red fluorescence and OD600
486 were measured using a Biotek H4 Synergy. **Solid:** Cells were diluted 1:100 from an
487 overnight culture into fresh LB and 20 µl plated onto individual wells in biological
488 triplicate in a 24 well plate with each well containing solidified 1.5% LB Agar with
489 antibiotics and inducer if required. The 24 well plate was then covered with a breathable
490 Aeraseal, and incubated at 37 ^{o}C with no shaking. At the indicated timepoint, cells were
491 harvested by flooding each well with 500 µl of M9 buffer, and were spun down at
492 8,000xg for 2 minutes, and resuspended in 500 µl of M9 media. Samples were loaded in
493 to a 96 well plate (150 µl /well) in technical triplicate and red fluorescence (excitation
494 580 nm, emission 610 nm) and OD600 were measured using a Biotek H4 Synergy. To
495 calculate the relative fluorescence units for each sample, the background fluorescence
496 and background OD600 values obtained were subtracted from the sample values, and
497 the sample fluorescence was then normalized to the sample OD600.
498
499 **AmrZ homolog discovery and characterization.** BLASTp was used to search the
500 nonredundant protein database for AmrZ homologs (accession: ABJ12639.1) in
501 *Pseudmonas sp.* (taxid: 286) in May 2019. This homolog list (e value > 0.001) was then
502 examined for homologs found on phage or plasmid genomes. Representative homologs
503 were aligned using Clustal and the alignment visualized in Jalview, and key conserved
504 residues were mapped onto the structure in Pymol (PDB ID: 3QOQ). Select homologs

were synthesized (TWIST Biosciences) and cloned into the SacI/PstI site of the arabinose-inducible plasmid pHERD30T using Gibson assembly. Vectors were electroporated into *Pseudomonas aeruginosa* strains for functional testing, where they were induced with 0.1% arabinose and maintained with 50 ug/mL gentimicin.

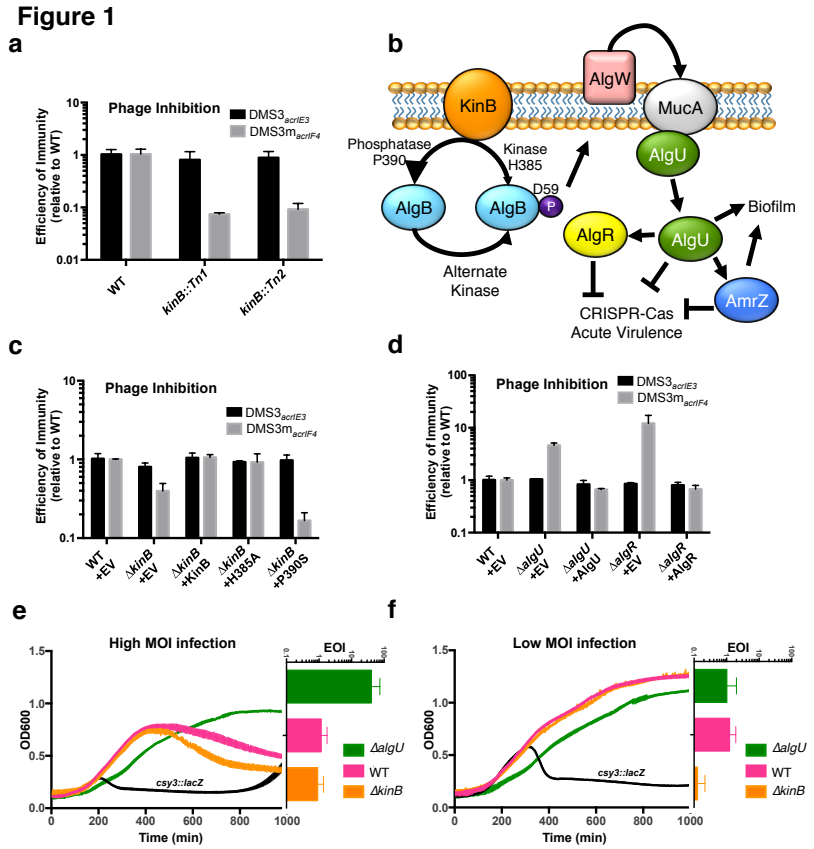

Figure 1: ***A forward genetic screen identifies a role for a biofilm activating pathway in repressing CRISPR-Cas immunity.*** **a**. Efficiency of immunity (EOI) against isogenic phages DMS3$_{acrIE3}$ (non-targeted) and DMS3m$_{acrIF4}$ (CRISPR-targeted). Plaque forming units (PFUs) were quantified on two independent *kinB* transposon mutants (*kinB::Tn1* and *kinB::Tn2*), then represented as a ratio relative to the number of PFUs measured on WT PA14. **b.** A cartoon summarizing the KinB/AlgB two component system and downstream effects, based on prior work, with CRISPR-Cas regulation added. **c**,**d** EOI measurements for indicated Δ*kinB,* Δ*algR,* and Δ*algU* strains with complementation. **e,f**. Growth curves of PA14 WT, Δ*algU*, or Δ*kinB* strains infected with either a high (e,10^6 PFU) or low (f, 10^4 PFU) MOI of virulent DMS3m$_{acrIF4}$. Phage

523 replication was quantified as PFUs after 24 hours, and the efficiency of immunity
524 expressed as a ratio of the number of PFUs harvested from the mutant strain compared
525 to the number of PFUs obtained from WT. All data (OD600 and EOI measurements) are
526 represented as the mean of 3 biological replicates +/- SD.

Figure 2

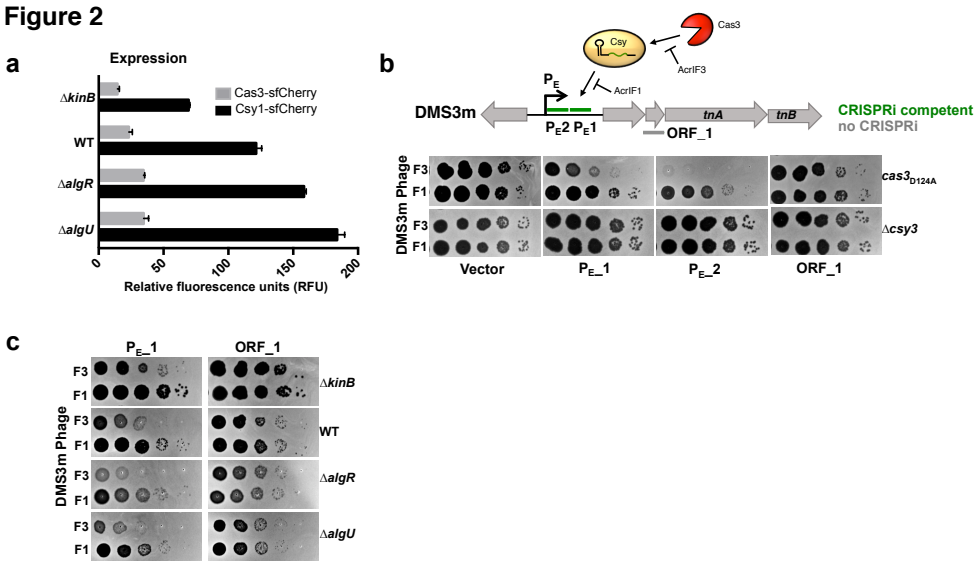

527

528 **Figure 2.** ***The kinB/algB pathway modulates Csy complex levels and activity.***
529 **a.** Measurement of the fluorescence levels of Cas3-sfCherry (grey) or Csy1-sfCherry
530 (black) reporter strains after 10 hours of growth in liquid culture. Fluorescence
531 measurements are represented as the mean of 3 biological replicates +/- SD. **b**. Spot
532 titration of DMS3m$_{acrIF3}$ (F3) and DMS3m$_{acrIF1}$ (F1) on *cas3*$_{D124A}$ (dead Cas3) or Δcsy3
533 (active Cas3, no Csy complex). Phages are targeted by natural spacer CR2_1, as well
534 as crRNAs designed to target DMS3m genome in positions designated on ORF map. **c**.
535 Spot titration of DMS3m$_{acrIF3}$ and DMS3m$_{acrIF1}$ phages on deletion mutants expressing
536 the indicated crRNA.
537

Figure 3

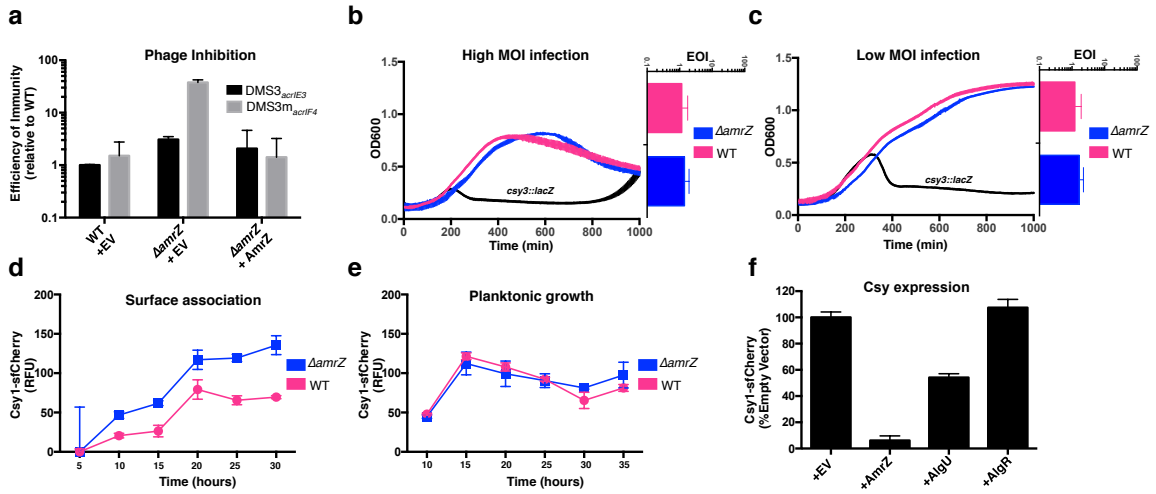

Figure 3: ***AmrZ is a surface-specific repressor of CRISPR-Cas immunity.***

a. Efficiency of immunity (EOI) against isogenic phages DMS3$_{acrIE3}$ (non-targeted) and DMS3m$_{acrIF4}$ (CRISPR-targeted). Plaque forming units (PFUs) were quantified on ΔamrZ or the complemented strain, then represented as a ratio of the number of PFUs measured on WT PA14. EOI measurements are represented as the mean of 2 biological replicates +/- SD. **b,c**. Growth curves of PA14 WT and Δ*amrZ* infected with either a high (d,10^6 PFU) or low (e, 10^4 PFU) MOI of virulent DMS3m$_{acrIF4}$. Phage replication was quantified as PFUs after 24 hours, and the efficiency of immunity expressed as a ratio of the number of PFUs harvested from Δ*amrZ* to the number of PFUs obtained from WT. OD600 and EOI measurements are represented as the mean of 3 biological replicates +/- SD. **d, e**. Timecourse of the fluorescence levels of Csy1-sfCherry reporter strains during surface-association (d) or planktonic growth (e). **f**. Overexpression of the indicated gene in a WT *csy1-sfCherry* background, with fluorescence measurements at 10 hours in liquid culture and normalized to empty vector. Fluorescence measurements are represented as the mean of 3 biological replicates +/- SD.

Figure 4

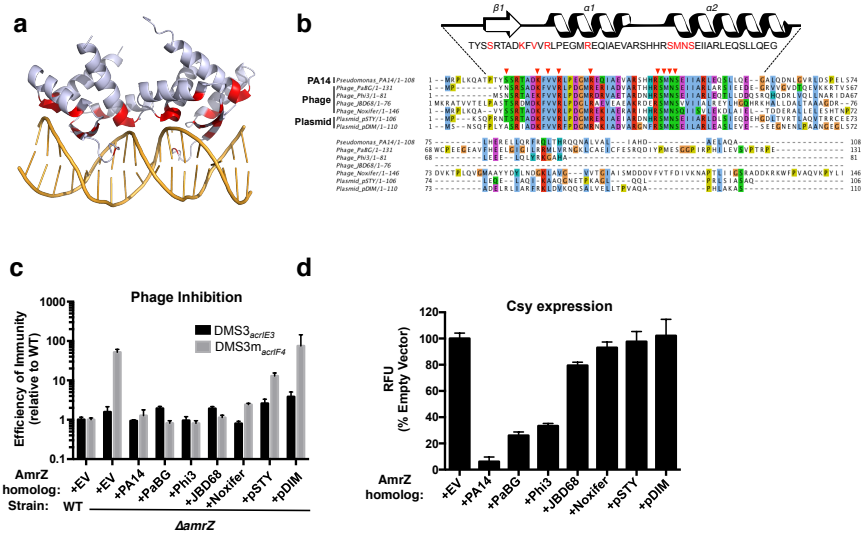

Figure 4. **Phage AmrZ homologs control CRISPR-Cas immunity. a.** Structure of an AmrZ tetramer bound to 18bp of operator DNA[58] with DNA-contacting residues highlighted in red. **b.** Protein alignment of six mobile AmrZ homologs and the native PA14 AmrZ homolog, with the ribbon-helix-helix DNA binding domain secondary structure schematized and DNA-contacting residues indicated with red arrows and text. **c.** Efficiency of immunity (EOI) against isogenic phages DMS3$_{acrIE3}$ (non-targeted) and DMS3m$_{acrIF4}$ (CRISPR-targeted). Plaque forming units (PFUs) were quantified on ΔamrZ or the strains complemented with bacterial or MGE AmrZ homologs, and represented as a ratio to the number of PFUs measured on WT PA14. EOI measurements as represented as the mean of 3 biological replicates +/- SD. **d.** Measurement of the normalized fluorescence levels of Csy1-sfCherry reporter strains transformed with bacterial or MGE AmrZ homologs after 10 hours of growth in liquid culture. Fluorescence measurements are represented as the mean of 3 biological replicates +/- SD.

Supplementary Table 1

Gene with Tn insertion	Transposon location	β-gal activity (% of unmutagenized)
kinB (1)	6448519	59%
kinB (2)	6447945	50%
kinB (3)	6447811	53%
kinB (4)	6449373	54%
kinB (5)	6449345	98%
purM	4618060	134%
lasR	4085810	135%
minD	1915545	N/D (growth defect)
gltB	5943637	108%
S-type pyocin	1196879	145%
pyoS3A	4404303	145%
tolA	4595505	158%
glycosyl transferase	5889967	81%
bacA	3490006	75%
Intergenic; zipA and smc +	3979746	N/D (growth defect)
gidB	6530337	88%
deaD	2373899	N/D (growth defect)
polA	6457284	N/D (growth defect)
pchH	798159	131%
crc	6275250	91%
putative plasmid stabilization protein	5347104	N/D (growth defect)
paraquat inducible protein	5532785	108%
pchH	797705	127%
yhiH/yhiI	6162134	108%
oxidoreductase FMN binding	4188602	N/D (growth defect)
putative membrane protein	1400718	118%
Intergenic; fstA and fstZ	5104077	111% (growth defect)
putative Zn-dependent oxidoreductase	2820446	115% (growth defect)
gnyL	3434168	87%
cytochrome c1 precursor	5126449	94%

569

570 **Supplementary Table 1**

571 All independent transposon insertions identified and mapped by visual screening with
572 increased or decreased *csy3::lacZ* β-galactosidase activity at 8 hours of growth. The
573 insertion location in the PA14 genome is shown, along with the measured level of β-
574 galactosidase enzyme. These measurements were not determined (N/D) for strains with
575 a growth defect.

Supplementary Table 2

Name	Accession	MGE type
PA14 AmrZ	ABJ12639.1	
Pseudomonas phage Noxifer	ARV77275.1	Lytic Myovirus
Pseudomonas phage phi3	YP_009276432.1	Integrated prophage
Pseudomonas phage PaBG	YP_008433620.1	Lytic Myovirus
Pseudomonas phage SM1	ALT58107.1	Siphoviridae (temperate)
Pseudomonas phage F10	YP_001293379.1	Siphoviridae (temperate)
Pseudomonas phage JBD68	ARM70500.1	Siphoviridae (temperate)
Pseudomonas sp. VLB120 plasmid pSTY	AGZ38169.1	Plasmid
Pseudomonas putida plasmid pKF715B	BAW27310.1	Plasmid
Pseudomonas veronii plasmid PVE_plasmid	SBW85251.1	Plasmid
Pseudomonas koreensis plasmid p3	AVX93364.1	Plasmid
Pseudomonas sp. Leaf58 plasmid pBASL58	AYG48213.1	Plasmid
Pseudomonas sp. XWY-1 plasmid	AUZ62175.1	Plasmid
Pseudomonas putida KF715C_pA870	BAW26592.1	Plasmid
Pseudomonas putida S12 plasmid pTTS12	AJA17154.1	Plasmid
Pseudomonas putida p12969-DIM	ALZ46341.1	Plasmid

Supplementary Table 2:

AmrZ homologs listed by the genome that encodes them, the accession number, and the mobile genetic element type.

Supplementary Figure 1

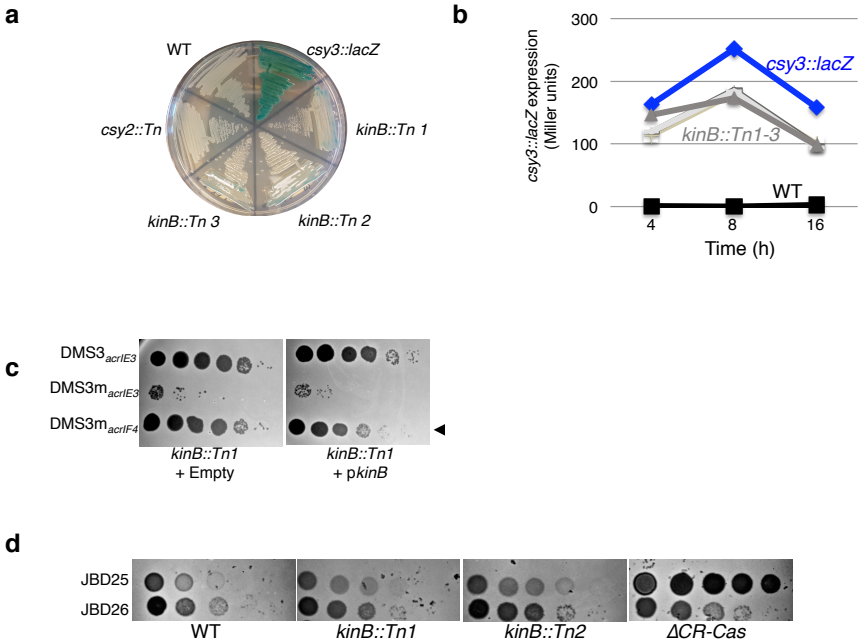

Supplementary Figure 1

a. A streak plate on X-gal plates, showing strains involved in this study and isolated transposon (Tn) insertions. **b**. β-galactosidase measurements at the indicated time points for the unmutagenized (*csy3::lacZ*) strain and three isolated *kinB* transposon mutants (*kinB::Tn1-3*). **c**. Phage titration on lawns of the *kinB::Tn1* mutant transformed with empty vector or *kinB.* **d.** Spot titration of phages JBD26 (CR2_sp17, sp20-targeted, possessing *acrIF4*), JBD25 (CR1_sp1 targeted) on *kinB::Tn* mutants and ΔCRISPR-Cas.

Supplementary Figure 2

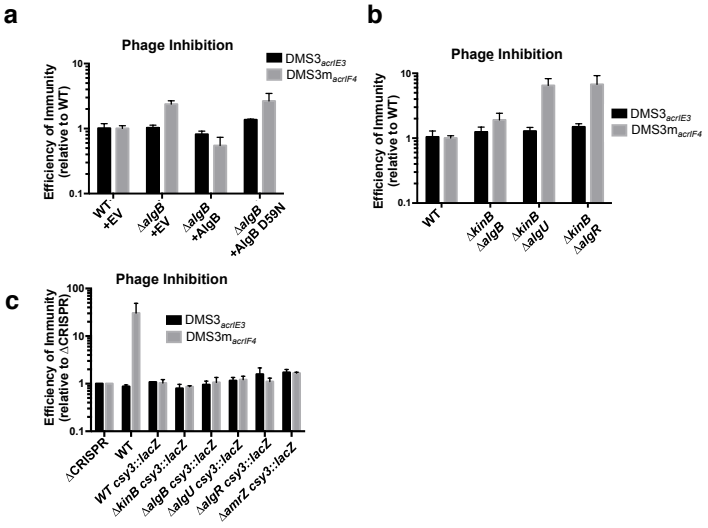

Supplementary Figure 2:

a-c. Efficiency of immunity measurements for indicated mutants relative to WT. **a**. Δ*algB* mutant complemented. **b.** Double knockouts show Δ*kinB* combined with *algB*, *algU*, or *algR*. **c**. Indicated knockouts were combined with *csy3::lacZ*.

Supplementary Figure 3

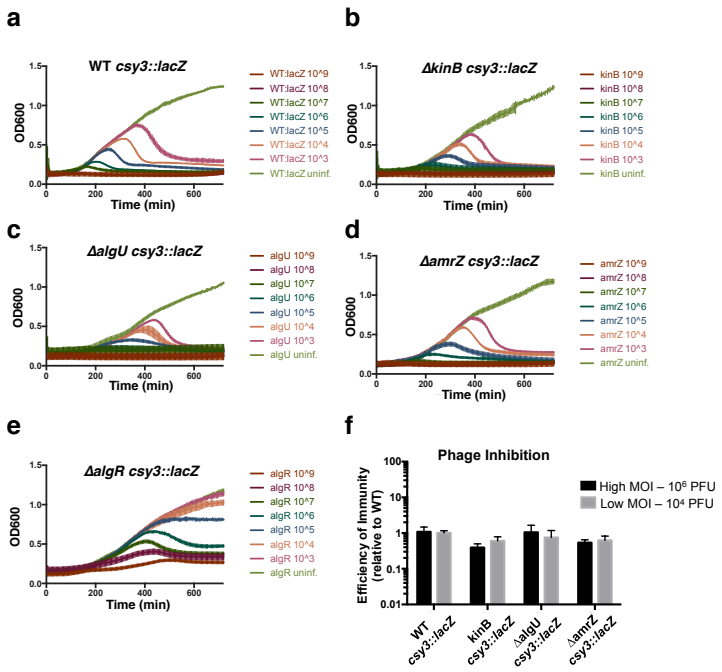

Supplementary Figure 3:

a-e. Growth curves of the indicated knockouts combined with *csy3::lacZ*. infected with virulent DMS3m$_{acrIF4}$ at multiplicity of infection (MOI, rainbow colors) increasing in 10-fold steps from $2x10^{-4}$ to $2x10^{2}$. **f.** Phage replication was quantified as PFUs after 24 hours for the MOIs used in Figure 1 and 3, and the efficiency of immunity expressed as a ratio of the number of PFUs harvested from the mutants combined with *csy3::lacZ* under the number of PFUs obtained from WT *csy::lacZ*. OD600 and EOI measurements are represented as the mean of 3 biological replicates +/- SD.

Supplementary Figure 4

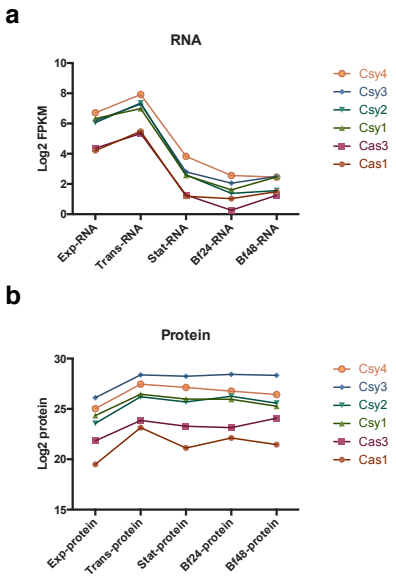

Supplementary Figure 4.

a. Log2 of Fragments Per Kilobase of transcript per Million mapped reads (FPKM) shown for each I-F *cas* gene in PA14 in the indicated growth condition. **b.** Log2 of protein levels for each of the I-F Cas proteins in PA14 in the indicated growth condition.

REFERENCES

1. Makarova, K. S. *et al.* An updated evolutionary classification of CRISPR-Cas systems. *Nat Rev Micro* **13,** 722–736 (2015).
2. Sapranauskas, R. *et al.* The Streptococcus thermophilus CRISPR/Cas system provides immunity in Escherichia coli. *Nucleic Acids Research* **39,** 9275–9282 (2011).
3. Vorontsova, D. *et al.* Foreign DNA acquisition by the I-F CRISPR-Cas system requires all components of the interference machinery. *Nucleic Acids Research* **43,** 10848–10860 (2015).
4. Mali, P. *et al.* RNA-guided human genome engineering via Cas9. *Science* **339,** 823–826 (2013).
5. Cong, L. *et al.* Multiplex Genome Engineering Using CRISPR/Cas Systems. *Science* **339,** 819–823 (2013).
6. Leon, L. M., Mendoza, S. D. & Bondy-Denomy, J. How bacteria control the CRISPR-Cas arsenal. *Curr Opin Microbiol* **42,** 87–95 (2018).
7. Patterson, A. G., Yevstigneyeva, M. S. & Fineran, P. C. Regulation of CRISPR-Cas adaptive immune systems. *Curr Opin Microbiol* **37,** 1–7 (2017).
8. Høyland-Kroghsbo, N. M. *et al.* Quorum sensing controls the Pseudomonas aeruginosa CRISPR-Cas adaptive immune system. *Proceedings of the National Academy of Sciences* **114,** 201617415–135 (2016).
9. Patterson, A. G. *et al.* Quorum Sensing Controls Adaptive Immunity through the

633 Regulation of Multiple CRISPR-Cas Systems. *Mol Cell* **64,** 1102–1108 (2016).
634 10. Høyland-Kroghsbo, N. M., Muñoz, K. A. & Bassler, B. L. Temperature, by
635 Controlling Growth Rate, Regulates CRISPR-Cas Activity in Pseudomonas
636 aeruginosa. *mBio* **9,** 1709–12 (2018).
637 11. Perez-Rodriguez, R. *et al.* Envelope stress is a trigger of CRISPR RNA-mediated
638 DNA silencing in Escherichia coli. *Molecular Microbiology* **79,** 584–599 (2011).
639 12. Serbanescu, M. A. *et al.* Role of the Streptococcus mutans CRISPR/Cas systems
640 in immunity and cell physiology. (2014). doi:10.1128/JB.02333-14
641 13. Shinkai, A. *et al.* Transcription activation mediated by a cyclic AMP receptor
642 protein from Thermus thermophilus HB8. *J. Bacteriol.* **189,** 3891–3901 (2007).
643 14. Patterson, A. G., Chang, J. T., Taylor, C. & Fineran, P. C. Regulation of the Type
644 I-F CRISPR-Cas system by CRP-cAMP and GalM controls spacer acquisition and
645 interference. *Nucleic Acids Research* **43,** gkv517–6048 (2015).
646 15. Agari, Y. *et al.* Transcription profile of Thermus thermophilus CRISPR systems
647 after phage infection. *Journal of Molecular Biology* **395,** 270–281 (2010).
648 16. Young, J. C. *et al.* Phage-induced expression of CRISPR-associated proteins is
649 revealed by shotgun proteomics in Streptococcus thermophilus. *PLoS ONE* **7,**
650 e38077 (2012).
651 17. Quax, T. E. F. *et al.* Massive activation of archaeal defense genes during viral
652 infection. *Journal of Virology* **87,** 8419–8428 (2013).
653 18. Fusco, S. *et al.* Transcriptome analysis of Sulfolobus solfataricus infected with two
654 related fuselloviruses reveals novel insights into the regulation of CRISPR-Cas
655 system. *Biochimie* (2015). doi:10.1016/j.biochi.2015.04.006
656 19. Brouns, S. J. J. *et al.* Small CRISPR RNAs guide antiviral defense in prokaryotes.
657 *Science* **321,** 960–964 (2008).
658 20. Hochstrasser, M. L. *et al.* CasA mediates Cas3-catalyzed target degradation
659 during CRISPR RNA-guided interference. *Proceedings of the National Academy*
660 *of Sciences* **111,** 6618–6623 (2014).
661 21. Westra, E. R. *et al.* CRISPR Immunity Relies on the Consecutive Binding and
662 Degradation of Negatively Supercoiled Invader DNA by Cascade and Cas3. *Mol*
663 *Cell* **46,** 595–605 (2012).
664 22. Levy, A. *et al.* CRISPR adaptation biases explain preference for acquisition of
665 foreign DNA. **520,** 505–510 (2015).
666 23. Cady, K. C., Bondy-Denomy, J., Heussler, G. E., Davidson, A. R. & O'Toole, G. A.
667 The CRISPR/Cas Adaptive Immune System of *Pseudomonas aeruginosa*
668 Mediates Resistance to Naturally Occurring and Engineered Phages. 1–40
669 (2012).
670 24. Haurwitz, R. E., Jinek, M., Wiedenheft, B., Zhou, K. & Doudna, J. A. Sequence-
671 and Structure-Specific RNA Processing by a CRISPR Endonuclease. *Science*
672 **329,** 1355–1358 (2010).
673 25. Wiedenheft, B. *et al.* Structural basis for DNase activity of a conserved protein
674 implicated in CRISPR-mediated genome defense. *Structure* **17,** 904–912 (2009).
675 26. Wiedenheft, B. *et al.* RNA-guided complex from a bacterial immune system
676 enhances target recognition through seed sequence interactions. *Proceedings of*
677 *the National Academy of Sciences* **108,** 10092–10097 (2011).
678 27. Rollins, M. F., Schuman, J. T., Paulus, K., Bukhari, H. S. T. & Wiedenheft, B.
679 Mechanism of foreign DNA recognition by a CRISPR RNA-guided surveillance
680 complex from Pseudomonas aeruginosa. *Nucleic Acids Research* (2015).
681 doi:10.1093/nar/gkv094
682 28. Rollins, M. F. *et al.* Cas1 and the Csy complex are opposing regulators of Cas2/3
683 nuclease activity. *Proceedings of the National Academy of Sciences* **23,**

684 201616395–E5121 (2017).
685 29. Chowdhury, S. *et al.* Structure Reveals Mechanisms of Viral Suppressors that
686 Intercept a CRISPR RNA-Guided Surveillance Complex. *Cell* **169,** 47–57.e11
687 (2017).
688 30. Zegans, M. E. *et al.* Interaction between bacteriophage DMS3 and host CRISPR
689 region inhibits group behaviors of Pseudomonas aeruginosa. *J. Bacteriol.* **191,**
690 210–219 (2009).
691 31. Cady, K. C. & O'Toole, G. A. Non-identity-mediated CRISPR-bacteriophage
692 interaction mediated via the Csy and Cas3 proteins. *J. Bacteriol.* **193,** 3433–3445
693 (2011).
694 32. van Belkum, A. *et al.* Phylogenetic Distribution of CRISPR-Cas Systems in
695 Antibiotic-Resistant Pseudomonas aeruginosa. *mBio* **6,** e01796–15 (2015).
696 33. Westra, E. R. *et al.* Parasite Exposure Drives Selective Evolution of Constitutive
697 versus Inducible Defense. *Curr. Biol.* **25,** 1043–1049 (2015).
698 34. van Houte, S. *et al.* The diversity-generating benefits of a prokaryotic adaptive
699 immune system. *Nature* **532,** 385–388 (2016).
700 35. Bondy-Denomy, J., Pawluk, A., Maxwell, K. L. & Davidson, A. R. Bacteriophage
701 genes that inactivate the CRISPR/Cas bacterial immune system. *Nature* **493,**
702 429–432 (2013).
703 36. Pawluk, A., Bondy-Denomy, J., Cheung, V. H. W., Maxwell, K. L. & Davidson, A.
704 R. A new group of phage anti-CRISPR genes inhibits the type I-E CRISPR-Cas
705 system of Pseudomonas aeruginosa. *mBio* **5,** e00896–e00896–14 (2014).
706 37. Bondy-Denomy, J. *et al.* Multiple mechanisms for CRISPR-Cas inhibition by anti-
707 CRISPR proteins. *Nature* **526,** 136–139 (2015).
708 38. Pawluk, A. *et al.* Inactivation of CRISPR-Cas systems by anti-CRISPR proteins in
709 diverse bacterial species. *Nature Microbiology* **1,** 1–6 (2016).
710 39. Cady, K. C. & O'Toole, G. Non-Identity-Mediated CRISPR-Bacteriophage
711 Interaction Mediated via the Csy and Cas3 Proteins. **193,** 3433–3445 (2011).
712 40. Cady, K. C., Bondy-Denomy, J., Heussler, G. E., Davidson, A. R. & O'Toole, G. A.
713 The CRISPR/Cas adaptive immune system of Pseudomonas aeruginosa
714 mediates resistance to naturally occurring and engineered phages. **194,** 5728–
715 5738 (2012).
716 41. Borges, A. L. *et al.* Bacteriophage Cooperation Suppresses CRISPR-Cas3 and
717 Cas9 Immunity. *Cell* **174,** 917–925.e10 (2018).
718 42. Damron, F. H. *et al.* Analysis of the Pseudomonas aeruginosa Regulon Controlled
719 by the Sensor Kinase KinB and Sigma Factor RpoN. **194,** 1317–1330 (2012).
720 43. Martin, D. W. *et al.* Mechanism of conversion to mucoidy in Pseudomonas
721 aeruginosa infecting cystic fibrosis patients. *Proc Natl Acad Sci USA* **90,** 8377–
722 8381 (1993).
723 44. Qiu, D., Eisinger, V. M., Rowen, D. W. & Yu, H. D. Regulated proteolysis controls
724 mucoid conversion in Pseudomonas aeruginosa. *Proc Natl Acad Sci USA* **104,**
725 8107–8112 (2007).
726 45. Chand, N. S. *et al.* The Sensor Kinase KinB Regulates Virulence in Acute
727 Pseudomonas aeruginosa Infection. **193,** 2989–2999 (2011).
728 46. Chand, N. S., Clatworthy, A. E. & Hung, D. T. The Two-Component Sensor KinB
729 Acts as a Phosphatase To Regulate Pseudomonas aeruginosa Virulence. **194,**
730 6537–6547 (2012).
731 47. Damron, F. H., Qiu, D. & Yu, H. D. The Pseudomonas aeruginosa Sensor Kinase
732 KinB Negatively Controls Alginate Production through AlgW-Dependent MucA
733 Proteolysis. **191,** 2285–2295 (2009).
734 48. Cezairliyan, B. O. & Sauer, R. T. Control of Pseudomonas aeruginosa AlgW

735 protease cleavage of MucA by peptide signals and MucB. *Molecular Microbiology*
736 **72,** 368–379 (2009).
737 49. Schurr, M. J., Yu, H., Martinez-Salazar, J. M., Boucher, J. C. & Deretic, V. Control
738 of AlgU, a member of the sigma E-like family of stress sigma factors, by the
739 negative regulators MucA and MucB and Pseudomonas aeruginosa conversion to
740 mucoidy in cystic fibrosis. *J. Bacteriol.* **178,** 4997–5004 (1996).
741 50. Tart, A. H., Blanks, M. J. & Wozniak, D. J. The AlgT-dependent transcriptional
742 regulator AmrZ (AlgZ) inhibits flagellum biosynthesis in mucoid, nonmotile
743 Pseudomonas aeruginosa cystic fibrosis isolates. *J. Bacteriol.* **188,** 6483–6489
744 (2006).
745 51. Baynham, P. J. & Wozniak, D. J. Identification and characterization of AlgZ, an
746 AlgT-dependent DNA-binding protein required for Pseudomonas aeruginosa algD
747 transcription. *Molecular Microbiology* **22,** 97–108 (1996).
748 52. Wozniak, D. J. & Ohman, D. E. Transcriptional analysis of the Pseudomonas
749 aeruginosa genes algR, algB, and algD reveals a hierarchy of alginate gene
750 expression which is modulated by algT. *J. Bacteriol.* **176,** 6007–6014 (1994).
751 53. Landsberger, M. *et al.* Anti-CRISPR Phages Cooperate to Overcome CRISPR-
752 Cas Immunity. *Cell* **174,** 908–916.e12 (2018).
753 54. Kong, W. *et al.* ChIP-seq reveals the global regulator AlgR mediating cyclic di-
754 GMP synthesis in Pseudomonas aeruginosa. *Nucleic Acids Research* **43,** 8268–
755 8282 (2015).
756 55. Lizewski, S. E. *et al.* Identification of AlgR-regulated genes in Pseudomonas
757 aeruginosa by use of microarray analysis. *J. Bacteriol.* **186,** 5672–5684 (2004).
758 56. Schulz, S. *et al.* Elucidation of sigma factor-associated networks in Pseudomonas
759 aeruginosa reveals a modular architecture with limited and function-specific
760 crosstalk. *PLoS Pathog* **11,** e1004744 (2015).
761 57. Wozniak, D. J. *et al.* Alginate is not a significant component of the extracellular
762 polysaccharide matrix of PA14 and PAO1 Pseudomonas aeruginosa biofilms.
763 *Proc Natl Acad Sci USA* **100,** 7907–7912 (2003).
764 58. Pryor, E. E. *et al.* The transcription factor AmrZ utilizes multiple DNA binding
765 modes to recognize activator and repressor sequences of Pseudomonas
766 aeruginosa virulence genes. *PLoS Pathog* **8,** e1002648 (2012).
767 59. Pratama, A. A. & van Elsas, J. D. A novel inducible prophage from the
768 mycosphere inhabitant Paraburkholderia terrae BS437. *Sci Rep* **7,** 9156 (2017).
769 60. Boucher, J. C., Yu, H., Mudd, M. H. & Deretic, V. Mucoid Pseudomonas
770 aeruginosa in cystic fibrosis: characterization of muc mutations in clinical isolates
771 and analysis of clearance in a mouse model of respiratory infection. *Infection and*
772 *Immunity* **65,** 3838–3846 (1997).
773 61. Martin, D. W., Holloway, B. W. & Deretic, V. Characterization of a locus
774 determining the mucoid status of Pseudomonas aeruginosa: AlgU shows
775 sequence similarities with a Bacillus sigma factor. *J. Bacteriol.* **175,** 1153–1164
776 (1993).
777 62. Damron, F. H., Qiu, D. & Yu, H. D. The Pseudomonas aeruginosa sensor kinase
778 KinB negatively controls alginate production through AlgW-dependent MucA
779 proteolysis. *J. Bacteriol.* **191,** 2285–2295 (2009).
780 63. Jones, A. K. *et al.* Activation of the Pseudomonas aeruginosa AlgU regulon
781 through mucA mutation inhibits cyclic AMP/Vfr signaling. **192,** 5709–5717 (2010).
782 64. Heilmann, S., Sneppen, K. & Krishna, S. Sustainability of virulence in a phage-
783 bacterial ecosystem. *Journal of Virology* **84,** 3016–3022 (2010).
784 65. Dötsch, A. *et al.* The Pseudomonas aeruginosaTranscriptional Landscape Is
785 Shaped by Environmental Heterogeneity and Genetic Variation. *mBio* **6,** e00749–

786 15–10 (2015).
787 66. Erdmann, J., Preusse, M., Khaledi, A., Pich, A. & Häussler, S. Environment-driven
788 changes of mRNA and protein levels in Pseudomonas aeruginosa. *Environmental*
789 *Microbiology* **20,** 3952–3963 (2018).
790